Supporting Information

Aluminum Macrocycles Induced Superior High-temperature Capacitive Energy Storage for Polymer-based Dielectrics via Constructing Charge Trap Rings

Zhongbin Pan[1], Yu Cheng[1], Zhicheng Li[1], Xi Pang[2], Peng Wang[3]*, Xu Fan[1], Hanxi Chen[4], Jinjun Liu[1], Junfei Luo[1]*, Jinghong Yu[4], Minhao Yang [5]*, Jiwei Zhai[3], and Weiping Li[6]*

[1]School of Materials Science and Chemical Engineering, Ningbo University, Ningbo, Zhejiang 315211, China. Email: luojunfei@ nbu.edu.cn

[2]State Key Laboratory of Electrical Insulation and Power Equipment, Xi'an Jiaotong University, Xi'an, Shaanxi 710049, P. R. China.

[3]School of Materials Science & Engineering, Tongji University, Shanghai, 201804 China. Email: dianlizi@126.com

[4]Key Laboratory of Marine Materials and Related Technologies, Zhejiang Key Laboratory of Marine Materials and Protective Technologies, Ningbo Institute of Materials Technology and Engineering, Chinese Academy of Sciences, Ningbo 315201, China.

[5]Institute of Energy Power Innovation, North China Electric Power University, Beijing, 102206, China E-mail: minhao.yang@ncepu.edu.cn

[6]School of Physical Sciences and Technology, Ningbo University, Ningbo, Zhejiang, 315211, China. E-mail: liweiping@nbu.edu.cn

This PDF file includes: Figures. S1 to S17, Note S1, and Table S1 to Table S2

Note S1 Space Charge Simulation

The bipolar transport model is used as the numerical simulation, including charge injection, charge migration, charge trapping, charge detrapping, charge recombination and charge extraction processes by using COMSOL Multiphysics version 6.0 with MUMPS and conjugate solver.

Charge transport can be described by the current continuity equation, the Poisson equation and the transport equation as follows:

$$\begin{cases} \dfrac{\partial n_a(x,t)}{\partial t} + \dfrac{\partial f_a(x,t)}{\partial x} = S_a(x,t) \\ \dfrac{\partial E(x,t)}{\partial x} = \dfrac{\rho_{all}(x,t)}{\varepsilon_0 \varepsilon_r} \\ f_a(x,t) = \mu_a(x,t) n_a(x,t) E(x,t) - eD_f \dfrac{dn}{dx} \end{cases}$$

where subscript a represents the types of carriers, including free electrons ($e\mu$), free holes ($h\mu$), trapped electrons (et) and trapped holes (ht); n_a is the carrier concentration, $C \cdot m^{-3}$; f_a is the carrier flux density, $A \cdot m^{-2}$; t is the time, s; x is the coordinate, m; ρ_{all} is the total charge density, $C \cdot m^{-3}$; μ_a is the mobility of carriers, $m^2 \cdot V^{-1} \cdot s^{-1}$; D_f is the diffusion coefficients, $m^2 \cdot s^{-1}$.

The variation of carrier i, $R_i(x, t)$, consisting of reactions between the bipolar charges during transport processes, which are as follows:

$$\begin{cases} S_{e\mu} = -S_1 \cdot n_{e\mu} \cdot n_{ht} - S_3 \cdot n_{e\mu} \cdot n_{h\mu} - B_e \cdot n_{e\mu} \cdot \left(1 - \dfrac{n_{et}}{N_{eto}}\right) + D_e \cdot n_{et} \\ S_{et} = -S_2 \cdot n_{et} \cdot n_{h\mu} - S_0 \cdot n_{et} \cdot n_{ht} + B_e \cdot n_{e\mu} \cdot \left(1 - \dfrac{n_{et}}{N_{eto}}\right) - D_e \cdot n_{et} \\ S_{h\mu} = -S_2 \cdot n_{et} \cdot n_{h\mu} - S_3 \cdot n_{e\mu} \cdot n_{h\mu} - B_h \cdot n_{h\mu} \cdot \left(1 - \dfrac{n_{ht}}{N_{hto}}\right) + D_h \cdot n_{ht} \\ S_{ht} = -S_1 \cdot n_{et} \cdot n_{h\mu} - S_0 \cdot n_{et} \cdot n_{ht} + B_h \cdot n_{h\mu} \cdot \left(1 - \dfrac{n_{ht}}{N_{hto}}\right) - D_h \cdot n_{ht} \end{cases}$$

where S_0, S_1, S_2 and S_3 is the recombination coefficient of trapped electron-trapped hole, free electron-trapped hole, trapped electron-free hole, and ree electron-free hole, $m^3 \cdot C^{-1} \cdot s^{-1}$; D_e and D_h

are the de-trapping coefficients of electron and hole, respectively, s^{-1}; N_{eto} and N_{hto} are the concentrations of electron traps and hole traps, respectively, $C \cdot m^{-3}$; B_e and B_h are the trapping coefficients of electron and hole traps, respectively, s^{-1}.

The source of charge in polymers (with the depth of D) is thought of as temperature-assisted injection from the electrodes at the state coordinate of (0,t) and (D,t), which is typically described by the Schottky law as follows:

$$\begin{cases} j_{ei}(0,t) = AT^2 \exp\left(\frac{-e\omega_{ei}}{kT}\right) \exp\left(\frac{e}{kT}\sqrt{\frac{e|E(0,t)|}{4\pi\varepsilon_0\varepsilon_r}}\right) \\ j_{hi}(D,t) = AT^2 \exp\left(\frac{-e\omega_{hi}}{kT}\right) \exp\left(\frac{e}{kT}\sqrt{\frac{e|E(D,t)|}{4\pi\varepsilon_0\varepsilon_r}}\right) \end{cases}$$

where ω_{hi} and ω_{ei} are the Schottky injection barriers for holes and electrons, respectively, eV; A is the Richardson constant to1.2×10^6 $A \cdot m^{-1} \cdot K^{-2}$; k is the Boltzmann constant to1.38×10^{-23} $J \cdot K^{-1}$.

During the transport process, hopping conduction between carriers in shallow traps is considered as follows:

$$\mu(x,t) = \frac{2v\lambda}{E(x,t)} \exp\left(\frac{-e\omega_{\mu}}{kT}\right) \sinh\left(\frac{eE(x,t)\lambda}{2kT}\right)$$

where $\mu(x,t)$ is the carrier mobility considering hopping conduction, $m^2 \cdot V^{-1} \cdot s^{-1}$; λ is the hopping distance, nm; ω_{μ} is the hopping barrier height, eV; v is the attempt-to-escape frequency, which is set to 6.7×10^{12} Hz. [S3]

The free charges can be trapped in deep traps with the trapping coefficients, which are described as follows:

$$B = \frac{\mu_a \cdot N_t \cdot e}{\varepsilon_0 \cdot \varepsilon_r}$$

where μ_a is the mobility of charges, $m^2 \cdot V^{-1} \cdot s^{-1}$; N_t is the trap density, m^{-3}; e=1.6×10^{-19} C, is the electronic charge.

Trapped charges can escape from deep traps by overcoming a potential barrier and the de-trapping

coefficient is as follows:

$$D = v \cdot \exp\left(\frac{-\Delta Utr}{k_B T}\right)$$

where ΔU_{tr} is the de-trapping barrier, eV, which is obtained from TSDC results.

The extraction of carriers at the electrode is assumed to be as normal conduction process with an extraction barrier as follows:

$$j_{e,h}(x,t) = n_{e\mu,h\mu}\mu_{e,h}E(x,t)$$

where j_e and j_h are the extraction current density of electrons and holes, respectively, $A \cdot m^{-2}$; $n_{e\mu}$ and $n_{h\mu}$ are the charge density of mobile electrons and holes, respectively; μ_e and μ_h are the mobilities of electrons and holes, respectively.

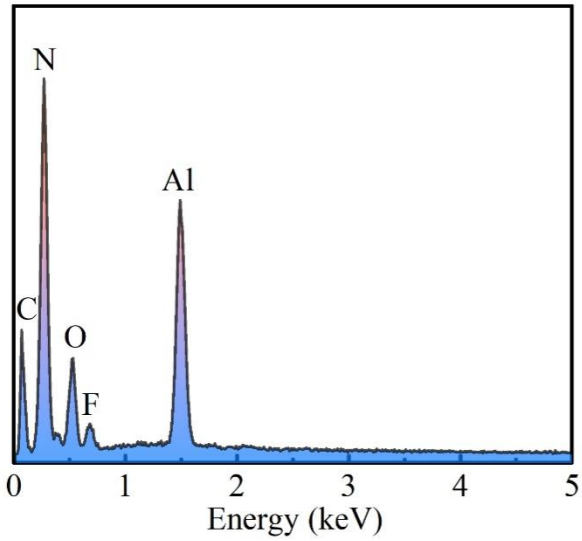

Figure S1 EDS spectra of AOC.

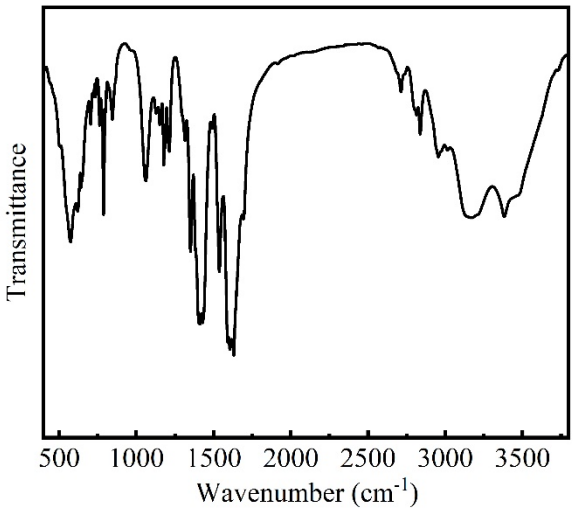

Figure S2 FT-IR spectra of AOC.

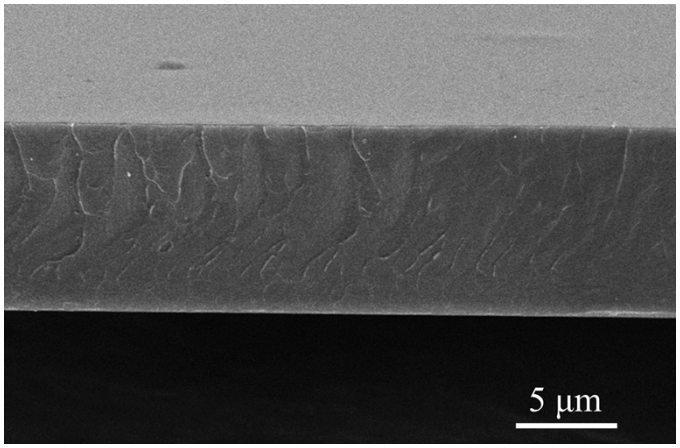

Figure S3 SEM of 0.5 wt.% AOC-PEI composite films.

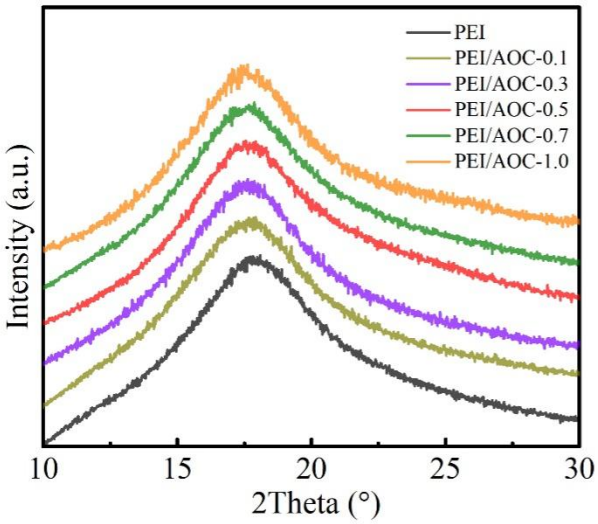

Figure S4 XRD patterns of PEI-AOC composite films.

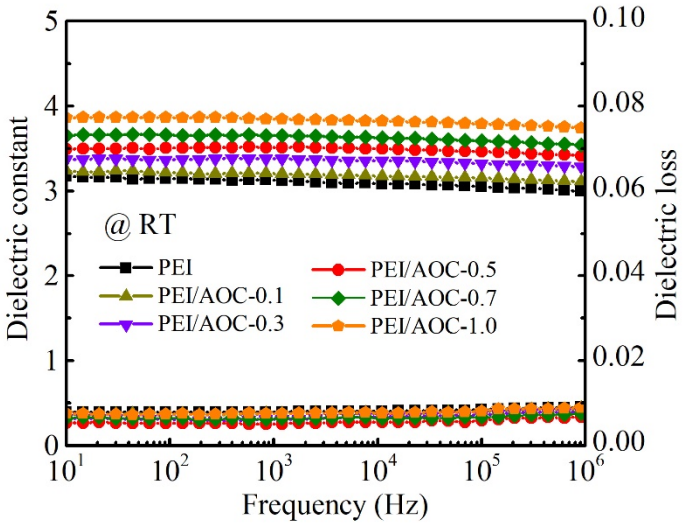

Figure S5 Dielectric constant and dielectric loss of pristine PEI and PEI-AOC composites at RT.

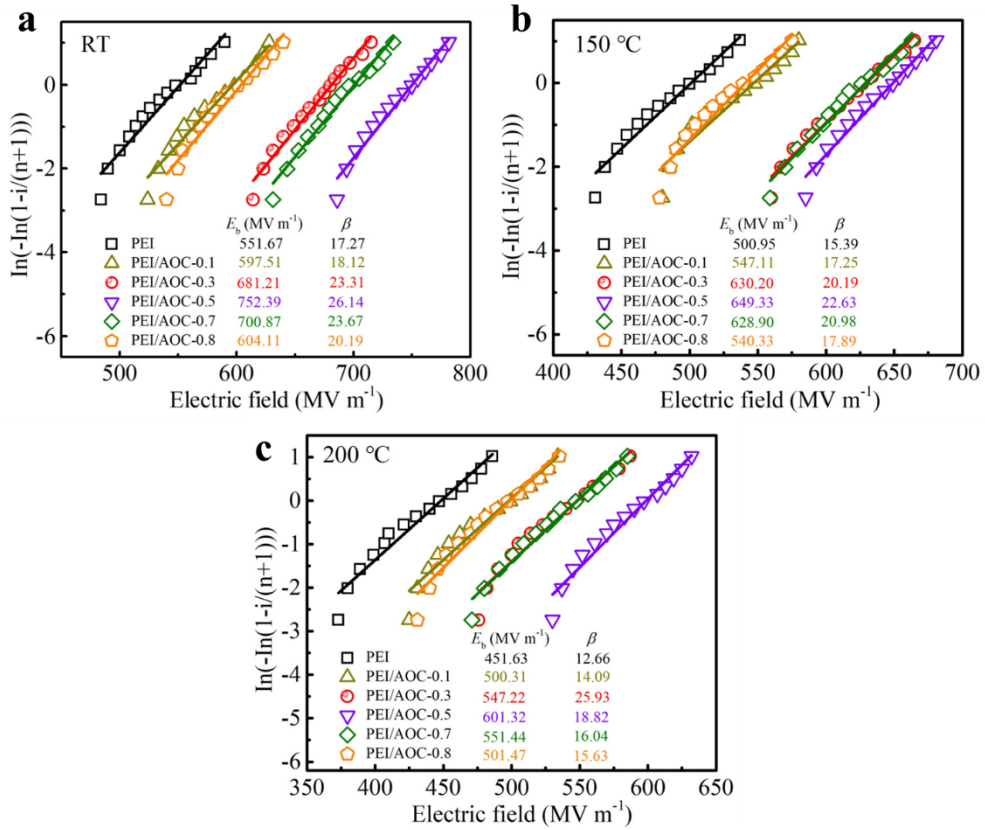

Figure S6 The dielectric breakdown strength and shape parameter of pristine PEI and PEI-AOC composites.

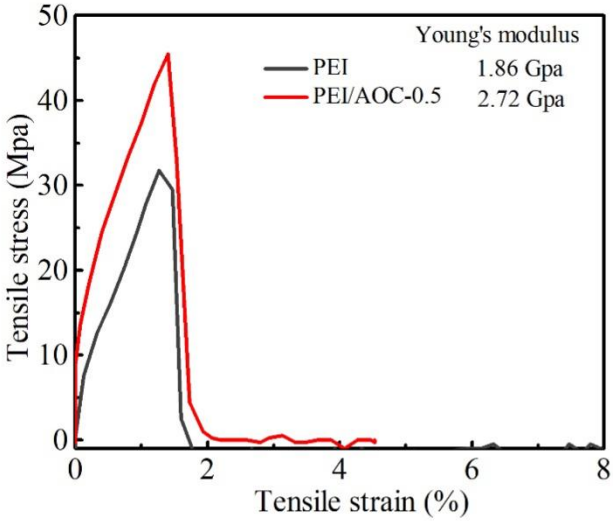

Figure S7 Tensile stress vs. tensile strain of pristine PEI and PEI-0.5 wt.% AOC composite.

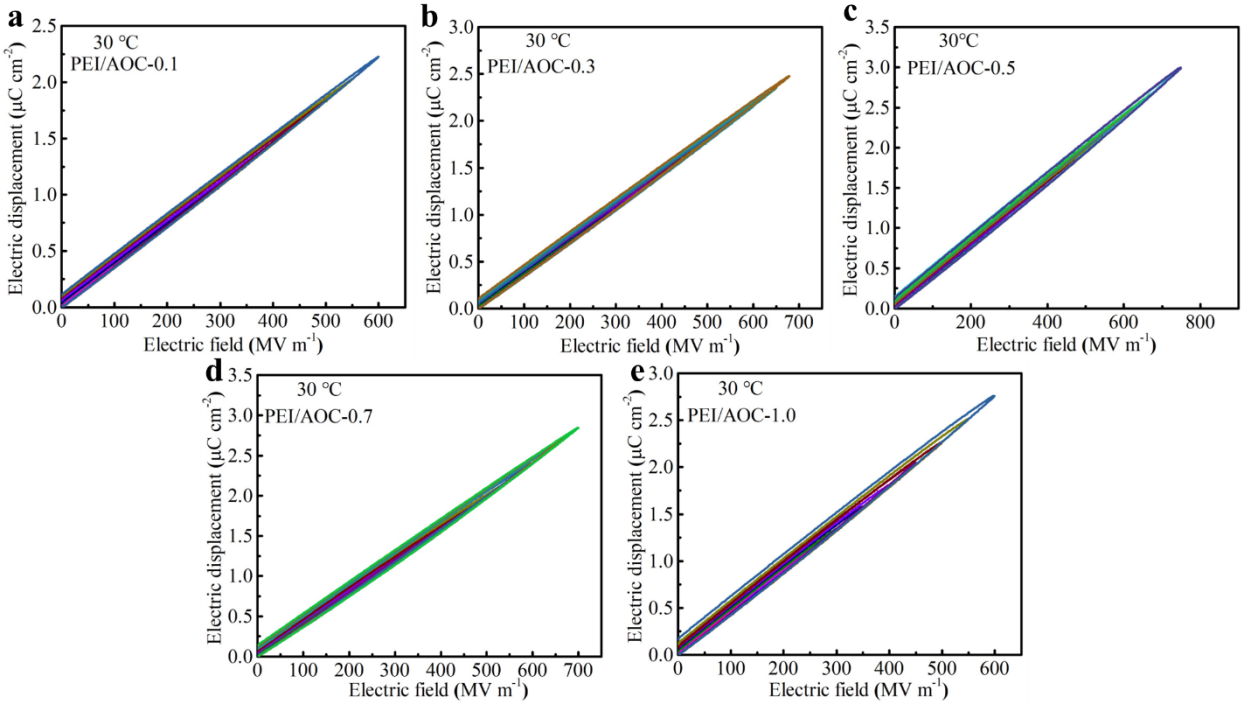

Figure S8 P-E curves of PEI-AOC composite with different contents of AOC at 30 °C.

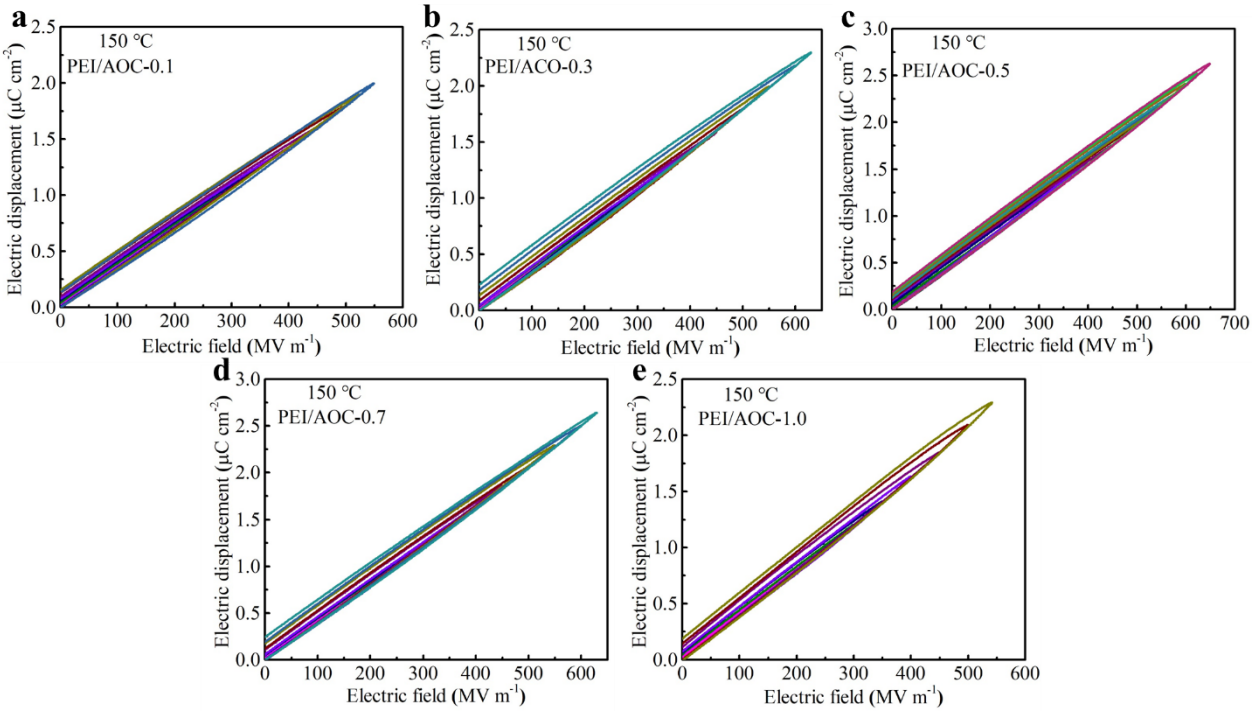

Figure S9 P-E curves of PEI-AOC composite with different contents of AOC at 150 ℃.

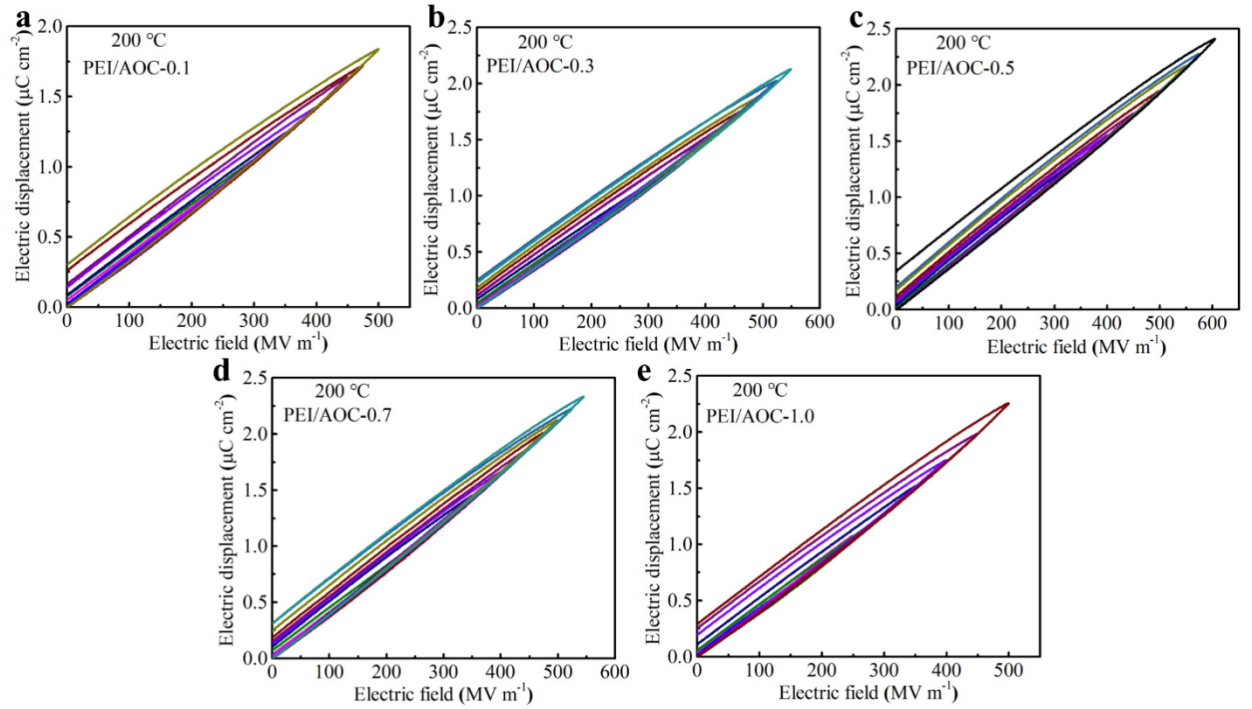

Figure S10 P-E curves of PEI-AOC composite with different contents of AOC at 200 ℃.

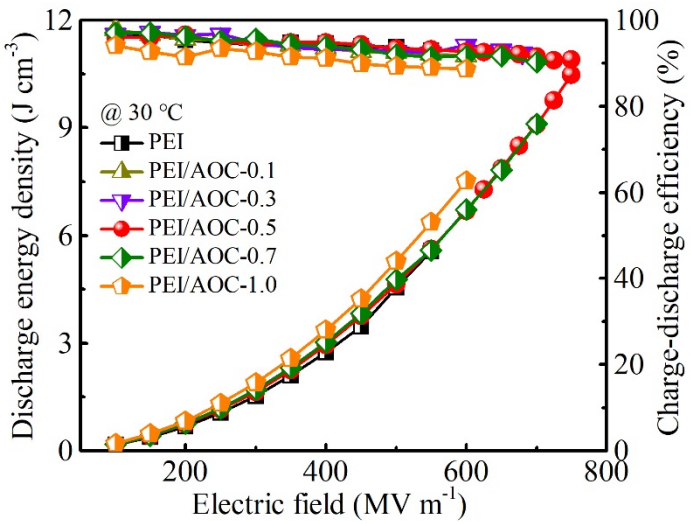

Figure S11 Discharged energy density and charge-discharge efficiency as function of electric field with PEI and PEI-AOC composite film at 30 ℃.

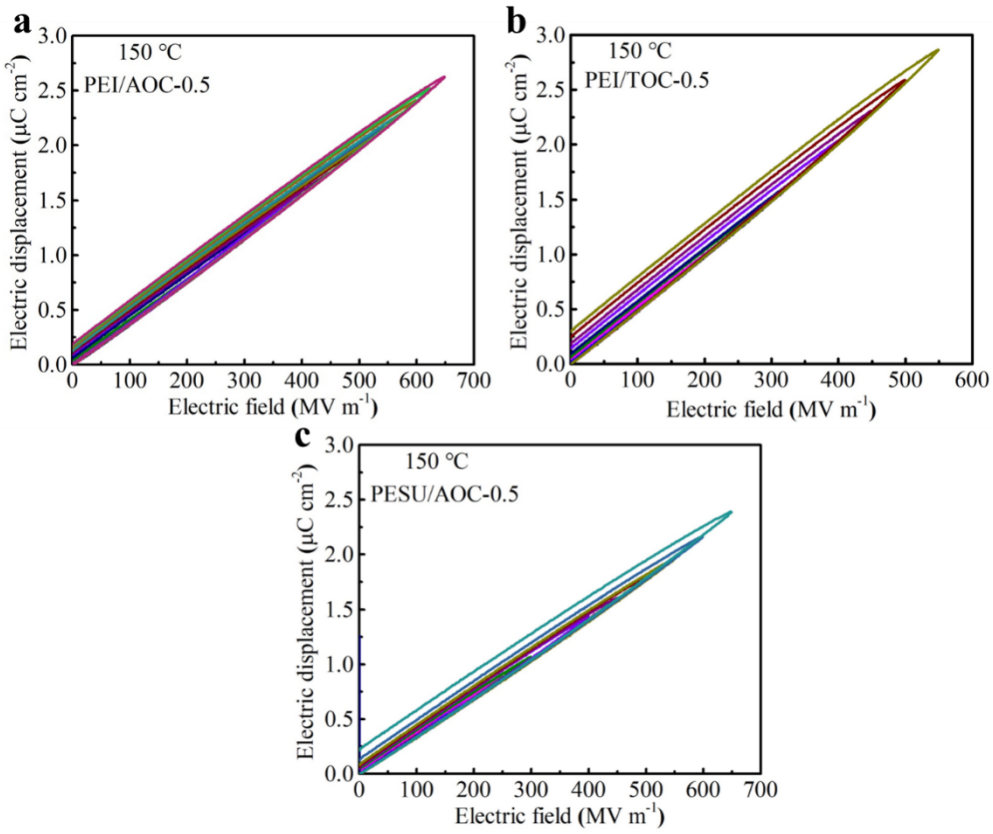

Figure S12 P-E curves of pristine PEI-AOC-0.5, PEI-TOC, and PESU-AOC composite at 150 ℃.

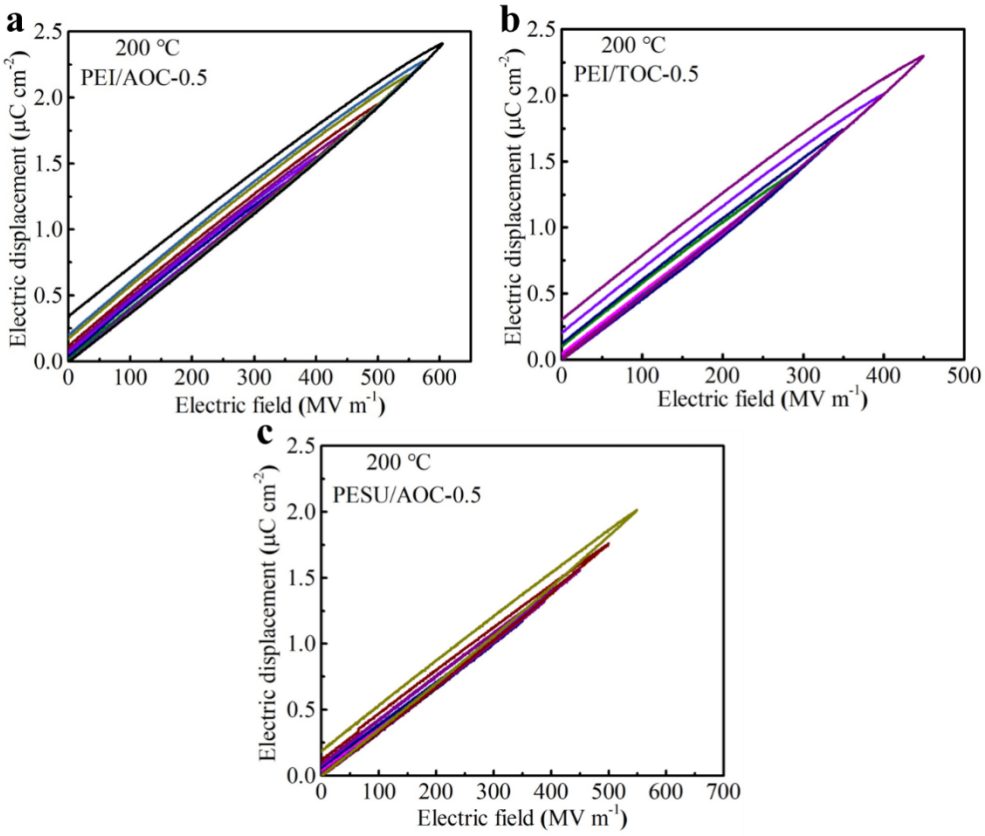

Figure S13 P-E curves of pristine PEI-AOC-0.5, PEI-TOC, and PESU-AOC composite at 200 ℃.

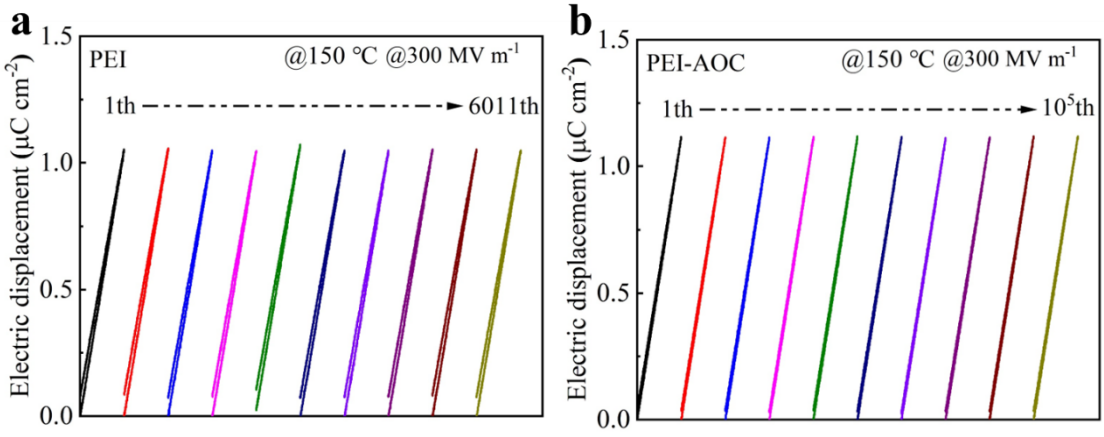

Figure S14 P-E curves of pristine PEI and PEI-AOC-0.5 composite with different charge-discharge cycles at 150 ℃.

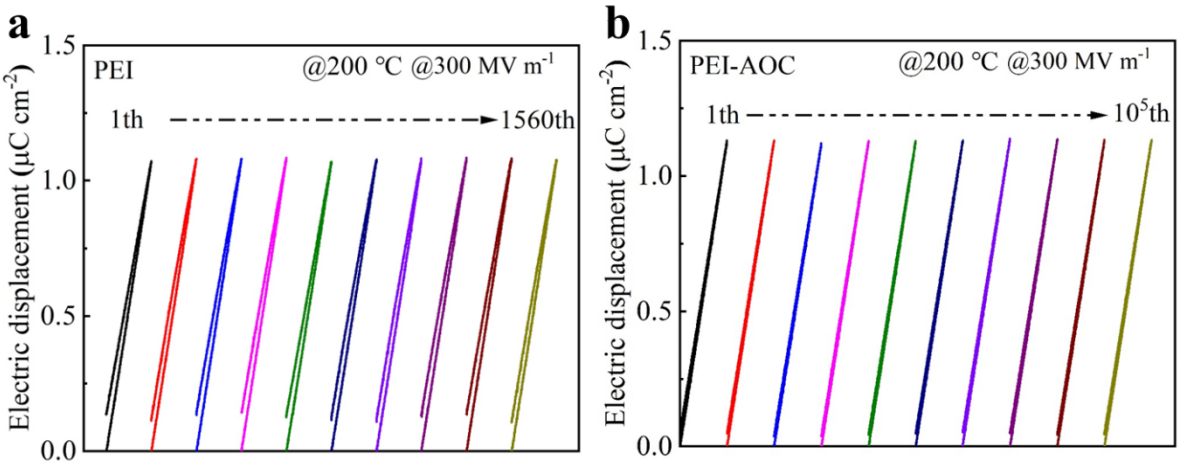

Figure S15 P-E curves of pristine PEI and PEI-AOC-0.5 composite with different charge-discharge cycles at 200 ℃.

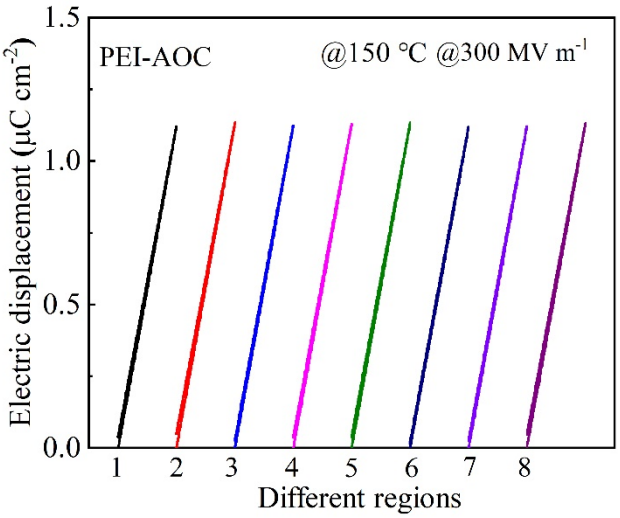

Figure S16 P-E curves of PEI-AOC-0.5 composite with different regions at 150 ℃.

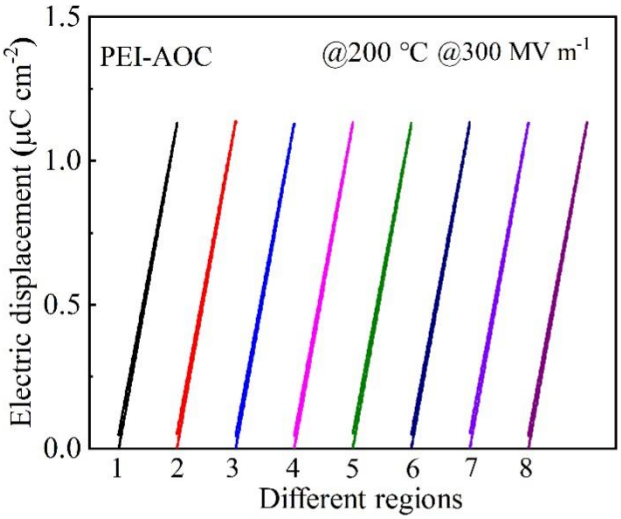

Figure S17 P-E curves of PEI-AOC-0.5 composite with different regions at 200 ℃.

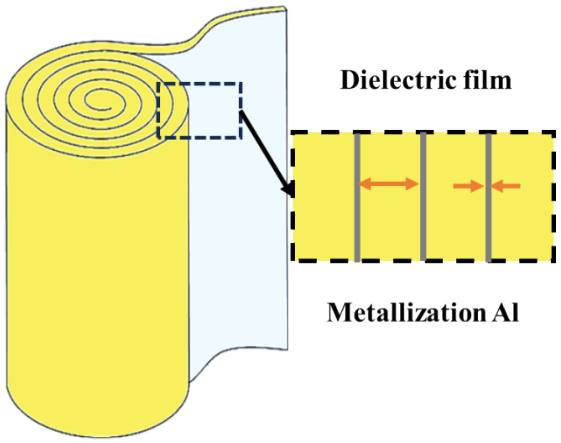

Figure S18 Winding capacitor model.

Table S1 Mulliken and Natural Population Analysis (NPA) charge analysis

Species	Mulliken charge (e)	NPA charge (e)	Species	Mulliken charge (e)	NPA charge (e)
Al	1.83	2.05	O	-0.51	-0.53
Al	1.97	2.09	O	-0.86	-1.05
Al	2.02	2.10	O	-0.53	-0.68
Al	2.02	2.04	O	-0.81	-1.02
Al	1.98	2.12	O	-0.86	-1.04
Al	1.99	2.10	O	-0.86	-1.04
Al	1.99	2.10	O	-0.51	-0.57
Al	1.96	2.08	O	-0.83	-1.02
Al	1.97	2.12	O	-0.86	-1.01
Al	1.98	2.12	O	-0.82	-1.02
O	-0.84	-1.03	O	-0.8	-0.97
O	-0.48	-0.62	O	-0.86	-1.05
O	-0.83	-1.04	O	-0.51	-0.56
O	-0.51	-0.58	O	-0.85	-1.04
O	-0.84	-1.04	O	-0.52	-0.69
O	-0.57	-0.68	O	-0.86	-1.01
O	-0.84	-1.06	O	-0.49	-0.58
O	-0.56	-0.67	O	-0.86	-1.04
O	-0.85	-1.04	O	-0.83	-1.02
O	-0.85	-0.99	O	-0.85	-1.05
O	-0.83	-0.99	O	-0.84	-1.00
O	-0.58	-0.70	O	-0.83	-1.03
O	-0.86	-1.00	O	-0.45	-0.58
O	-0.85	-1.00	O	-0.84	-1.03
O	-0.83	-1.04	O	-0.83	-1.00

Table S2 Charge-discharge cycles compared with other state-of-the-art polymer composite.

Dielectric Materials	**Charge-Discharge Cycles**	**Ref.**
P(VDF-HFP)-AO NPLs	> 50,000	Adv. Funct. Mater. 2021, 31, 2006739.
P(VDF-HFP)-GLC	> 50,000	Energy Storage Mater. 2022, 49, 339.
*c*BCB-*co*-SNI	>50,000	Energy Environ. Sci., 2024, 17, 8866.
PEI/HEnf	>50,000	Adv. Energy Mater. 2023, 13, 2203925.
PEI/PEEU	>20,000	J. Power Sources 2023, 570, 233053.
PEI/UiO-66-F4	>100,000	Energy Environ. Sci., 2025, 18, 620.
E-c-SiO_2 NPs/PEI	>50,000	Adv. Energy Mater. 2025, 2405411.
FPI-TE	>100,000	Adv. Mater. 2023, 35, 2302392.
FPI-DG	>50,000	Nat. Commun. 2024, 15, 8647.
PS-*b*-P4VP(PDP)-ZrO_2	>50,000	Adv. Mater. 2024, 36, 2401954.
Polysulfate P6	>100,000	Nature Energy 2025, 10, 90.
BNKT-BST/PEI	>10,000	Adv. Mater. 2025, 37, 2415652.
PEI-AOC	**>100,000**	**This work**